MISIRoot: A Robotic Minimum Invasion in Situ Imaging System for Plant Root Phenotyping

Zhihang Song [1], Wei Qiu [2*], Jian Jin [1*]

[1] Department of Agricultural and Biological Engineering, Purdue University, West Lafayette, IN 47907, United States

[2] College of Engineering, Nanjing Agricultural University, Nanjing, China

Corresponding authors:

*Wei Qiu

Associate Professor, College of Engineering, Nanjing Agricultural University

Address: Nanjing Agricultural University, PuKou, Nanjing, 210031, China

Phone: +86 15850724893

E-mail: qiuwei@njau.edu.cn,

*Jian Jin

Assistant Professor, Department of Agricultural and Biological Engineering, Purdue University

Address: 225 South University Street, West Lafayette, IN 47907, United States

Phone: +1 (765) 494-1182

E-mail: jinjian@purdue.edu

Abstract

Background: Plant root phenotyping technologies play an important role in breeding, plant protection, and other plant science research projects. The root phenotyping customers urgently need technologies that are low-cost, in situ, non-destructive to the roots, and suitable for the natural soil environment. Many recently developed root phenotyping methods such as minirhizotron, X-CT, and MRI scanners have their unique advantages in observing plant roots, but they also have disadvantages and cannot meet all the critical requirements simultaneously.

Results: The study in this paper focuses on the development of a new plant root phenotyping robot that is minimally invasive to plants and working in situ inside natural soil, called "MISIRoot". The MISIRoot system mainly consists of an industrial-level robotic arm, a mini-size camera with lighting set, a plant pot holding platform, and the image processing software for root recognition and feature extraction. MISIRoot can take high-resolution color images of the roots in soil with minimal disturbance to the root and reconstruct the plant roots' three-dimensional (3D) structure at an accuracy of 0.1 mm. In a test assay, well-watered and drought-stressed groups of corn plants were measured by MISIRoot at V3, V4, and V5 stages. The system successfully acquired the RGB color images of the roots and extracted the 3D points cloud data containing the locations of the detected roots. The plants measured by MISIRoot and plants not measured (control) were carefully compared with the results from the Hyperspectral Imaging Facility (reference). No significant differences were found between the two groups of plants at different growth stages.

Conclusion: The MISIRoot system recently developed at Purdue University has been proved effective in root phenotyping with multiple advantages: With a comparatively low cost and

minimal invasion to the plant, this system can automatically measure the root's 3D structure and take color images of the roots in ordinary soil media, and in situ. This system provides a new option for root phenotyping researchers and has a potential to be applied in a wide range of research topics such as breeding, plant protection and so on.

Keywords:

Plant root phenotyping, root imaging, 3D point cloud, minimally invasive root measurement, low-cost root phenotyping, robotic arm application

Background

Plant phenotyping technology has been playing an important role in assisting researchers studying the connections between plant phenotypes and genotypes (1). This technology can monitor the plant's physical growing condition (2), predict nutrient deficiencies (3), and detect plant diseases (1). Plant root is a type of organ that mostly grows in the soil, which works to acquire water and nutrients from the living environment (4,5), sense the environment(6), and forward sensing messages to the plant body (7). In addition, the root network is the base foundation that supports the above-ground plant body to stand firmly (8) and to withstand natural hazard like strong wind and drought stress (8,9). Thus, studying the plant root phenotypes is critical for learning more about plant growing health, bidirectional influences between soil content effect and plant roots, and symbiotic relationship between root and Rhizobia (De Baets et al., 2008; Cheol Song et al., 2016).

However, development of root phenotyping methods severely falls behind the demands from plant researchers due to many challenges including: 1) Plant roots are naturally growing

in opaque soil, which makes it difficult to directly image root. 2) Unlike the stem and leaves structure of a plant that are above the ground, it is hard to detect the complex 3-dimensional morphological patterns of underground roots. 3) The complexity of soil environment and the softness of root body makes it difficult to measure roots in a non-destructive way or in situ.

In recent years, researchers have developed several progressive methods that could overcome certain aspects of challenges for plant root phenotyping. For example, growing the plants in a transparent medium offers the convenience for researchers to image the plant roots directly without being blocked by the opaque soil (12,13). However, the gel-based or liquid-based medium can be far from comparable with the real natural soil. As a result, plant roots could grow differently in those two mediums because of soil's differences in physical, chemical and biological characteristics. In a currently popular type of method called "minirhizotron" (14–16), researchers buried transparent plastic tubes with camera or deployed several miniature cameras directly into soil, and then waited for the roots to come close enough for being imaged (16). Minirhizotron has the advantages that it can measure the root structure in situ and with natural soil. However, with the hard materials like plastic tubes or circuit boards buried in the soil, plant roots can be misled and redirected off their original growing paths. As a result, the root poses that the plant was intended to grow may be lost. Other most recent technologies such as X-ray Computed Tomography (X-CT) (17,18) and Magnetic Resonance Imaging (MRI) can provide high resolution 3D data of the plant root structures in natural soil (19), and overcome most of the challenges described above (20). However, there are still unsolved major challenges that could prevent most of the researchers from being able to use these technologies. X-CT and MRI system typically have: 1) extremely high price for both software and hardware system, 2) large system size which makes it hard to be constructed or transported, 3) a challenge that the data quality could be dramatically influenced by the properties of soil (21), 4) safety-risky usage of radioactive materials in X-CT, and 5) safety-risky usage of strong magnet in MRI.

Since all these methods have their unique advantages but also disadvantages, researchers are demanding a better solution that can overcome as many challenges as described above.

This paper introduces a relatively low-cost and easy-to-implement method that can collect color digital images of the plant roots within the original soil environment and reconstruct the 3D structure of the root without damaging the roots or changing their original poses. This method utilizes an industrial level robotic arm to hold a miniature camera and repeatedly inserting the camera into the soil to certain positions while recording frames with 3D coordinates of each image. The real-world implementation of this method is called 'MISIRoot' in this paper. In the most recent experiment, it successfully generated a 3D point cloud of a corn plant and collected many high-resolution 3D-positioned color images of the plant roots. The point cloud can help researchers measure the morphological features of the plant root in terms of depth, width, density distribution and so on. The roots' surface texture and their living environment in the soil can be clearly observed from the color images.

Materials and methods

In general, MISIRoot takes several color images (RGB) on corn plant roots by controlling a robotic arm to insert a mini-size RGB camera into the soil media where the corn root exists. It records the Cartesian X, Y, and Z coordinates of the camera tip position when taking each image. All the images and coordinates data are directly saved into the computer's hard disk as Portable Network Graphic (PNG) and Comma-Separated Values (CSV) files respectively, which could be easily accessed for further processing. A software program was developed to process the images and their positions data to calculate various root feature results.

A provisional patent application was filed by Purdue University for the design of the MISIRoot system in 2019.

1. Hardware system design

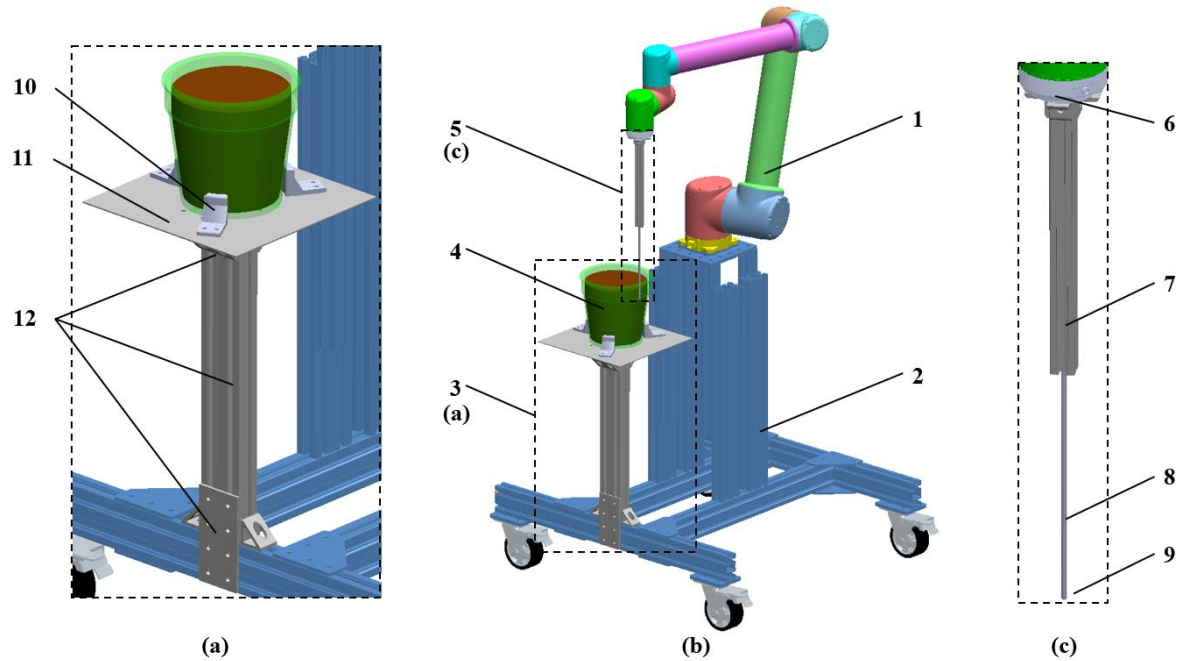

Fig. 1. Hardware system design of the MISIRoot system

(a) Detailed view of component No. 3, (b) MISIRoot system overview, (c) Detailed view of component No. 5.

1. Robotic arm (Universal Robot Inc., UR10)

2. System base (Vention Inc., Aluminum frames)

3(a). Experiment platform (10. Pot clamp, 11. Support panel, 12. Support frames)

4. Virtual plant pot in position

5(c). Imaging head (6. Mounting panel, 7. Aluminum T-slotted frame, 8. Stainless-steel tube, 9. Endoscope camera head)

The system was carefully designed to capture root images of a plant in the soil with minimum impact to the plant's growth. MISIRoot continuously takes measurements automatically by inserting a tiny camera facing vertically downwards to capture images near the plant roots. Fig. 1 shows the design of the hardware system which consists of four main

components, including a robotic arm, a system base, an experiment platform, and an imaging head.

1.1. Robotic Arm and system base

The robotic arm works as one of the most important components of the MISIRoot system. The robotic arm, which is UR10 (Universal Robots Inc.), was carefully chosen to meet many requirements of the system design. Some of the key specifications of this robotic arm are listed in the Table 1. In terms of the hardware, it has enough payload and power for holding and stabbing the imaging head into soil, enough moving speed to ensure high throughput, enough movement range to cover the whole sampling region, and enough degrees of freedom for taking measurements at specific gestures. As for the software, it has an accurate control system to minimize the measurement errors when the robotic arm repeatedly performs inserting and pulling actions. It has a high-frequency feedback system for sending position and counter-acting force information to the user interface, which helps the researcher record the 3D coordinates of each image and check the system's real-time status. In the MISIRoot system, a virtual boundary and a force limit was set in the UR10 control system so that if the robotic arm moves out of the safety range or encounters a force larger than 10 newtons, the system would be emergently stopped.

System base is a compact base structure mainly consisting of multiple aluminum extrudes, connection parts, and wheels. It serves as a stable supporting platform during experiments and the system can be easily transported between the research lab and the greenhouse with its wheels.

147 **Table 1.** Technical specifications of the UR10 robotic arm.

Specifications	values
Weight	28.9 kg / 63.7 lbs.
Payload	10 kg / 22 lbs.
Reach	1300 mm / 51.2 in
Join ranges	+/- 360°
Speed	Base and shoulder: 120 °/s. Elbow and wrists:180 °/s. Tool: typical 1 m/s / 39.4 in/s
Repeatability	+/- 0.1 mm / +/- 0.0039 in (4 miles)
Degrees of freedom	6 rotating joints
Communications	TCP/IP 100Mbit: IEEE 802.3u, 100BASE-TX Ethernet socket & Modbus TCP
Programming	Universal Robots Software (PolyScope) graphical user interface on 12 in touch screen with mounting
International protection classification	IP54
Working temperature	0 – 50 °C

148

149 1.2. Experiment platform

150 Since the MISIRoot system records the 3D coordinates of the imaging head while
151 taking each image, a 3D cartesian coordinate system was established for the system. Referring
152 to Fig. 1., the main vertical beam is a 45 mm × 90 mm T-slotted frame (McMaster-Carr Inc.),
153 mounted firmly on the system base. Located at the top of the main beam, is a 7075-aluminum

square shape panel and a set of pot clamps designed so that the plant pot can be easily and firmly mounted at a proper position.

1.3. Imaging head

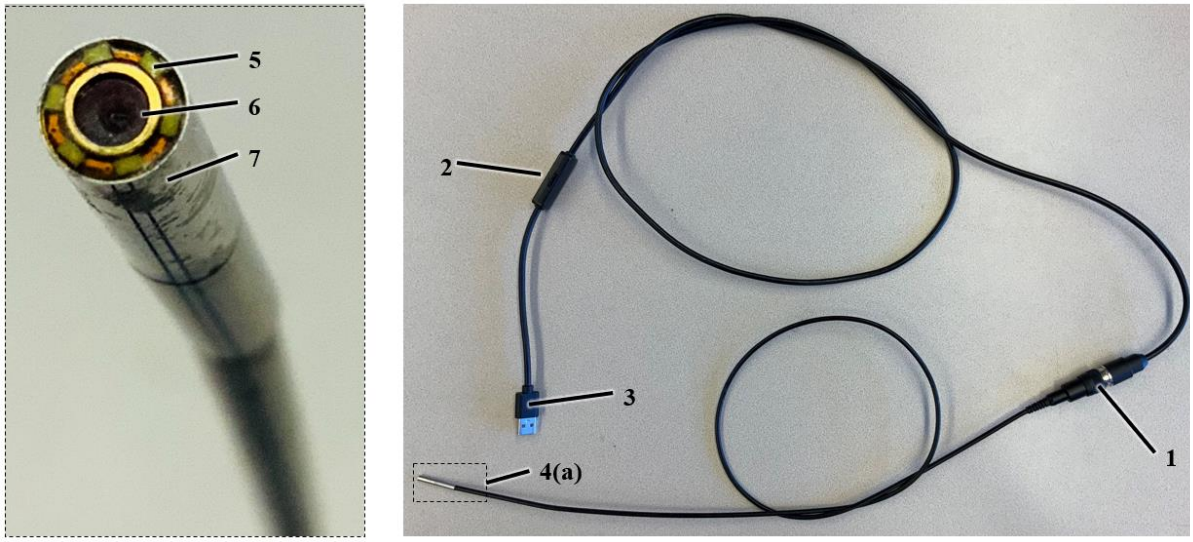

Fig. 2. Endoscope camera with cable, cable converter, and LED brightness controller.

(a) Detailed view of the camera head, (b) Overview of the endoscope camera.

1. Camera cable to USB 2.0 converter

2. LED brightness controller

3. USB 2.0 (male)

4(a). Camera head (5. A ring of 6 LEDs, 6. Camera and lens, 7. Stainless-steel cover)

As shown in Fig. 2., the imaging head consists of an aluminum T-slotted frame, a stainless-steel tube, and an endoscope camera with its cable going through the stainless-steel tube. As the most important component of this subsystem, the endoscope camera was carefully selected and redesigned by outside service based on many requirements of MISIRoot's system design. First, the size (diameter) of the camera should be as small as possible, so that the measurement impact on soil environment can be minimized. The camera chosen in MISIRoot

has a diameter of 3.95 mm, which is comparable with the size of a typical earthworm. Second, the camera's pixel resolution is 640 × 480, which is clear enough for researchers to view plant roots in the 5 mm diameter tunnel created by the camera head. Third, the camera head is equipped with a set of 6 white Light-Emitting Diodes (LEDs), which ensures the visibility when working inside the soil. The LEDs are bright enough that the exposure time can be set to lower than 1/60 seconds to avoid blurry images. Because of LEDs' characteristic of low-power-consumption, the lights do not generate significant heat and will not burn the roots. Fourth, the camera head is tightly wrapped with a 5 mm outer-diameter stainless-steel tube for protecting the lens when being inserted into soil. Fifth, the camera has a fixed focal length, a fixed aperture size and a small field of view. For an object in an image to be well focused, the distance between the object and the camera's tip should be 3 mm. Thus, if the image contains a root with clear edges, it means that the root is 3 mm away from the camera tip. As the 3D position and 3-axial directions of the camera tip are known, the position of detected root can be calculated accordingly.

Table 2. Technical specifications of the endoscope camera

Specifications	**values**
Total length	2520 mm
Length of the metal cover	28.3 mm
Camera head diameter	3.95±0.05 mm
Stainless-steel tube size	4.39 mm inside diameter, 5.16±0.003 mm outside diameter
Censor resolution	640 × 480 pixels
Censor type	RGB CCD

Focal Length	4 mm
Total power consumption	5V 200mA
Communication protocol	USB 2.0 Serial
Light source	6 × white LED
International protection classification	IP54

2. System control program design

The control logic and data flow diagram are shown in Fig. 3. Overall, there are 3 major subsystems including the MISIRoot base, a UR10 control box, and a desktop computer. The core control program was written in Python (3.7), running on a computer with Linux (Ubuntu 16.04) operating system. The UR10 control box came with the UR10 robotic arm when purchasing. In this system setup, the control box was connected to the robotic arm for both sending control signals and accepting feedback data. The desktop computer communicates with the control box through an ethernet cable with TCP/IP protocol.

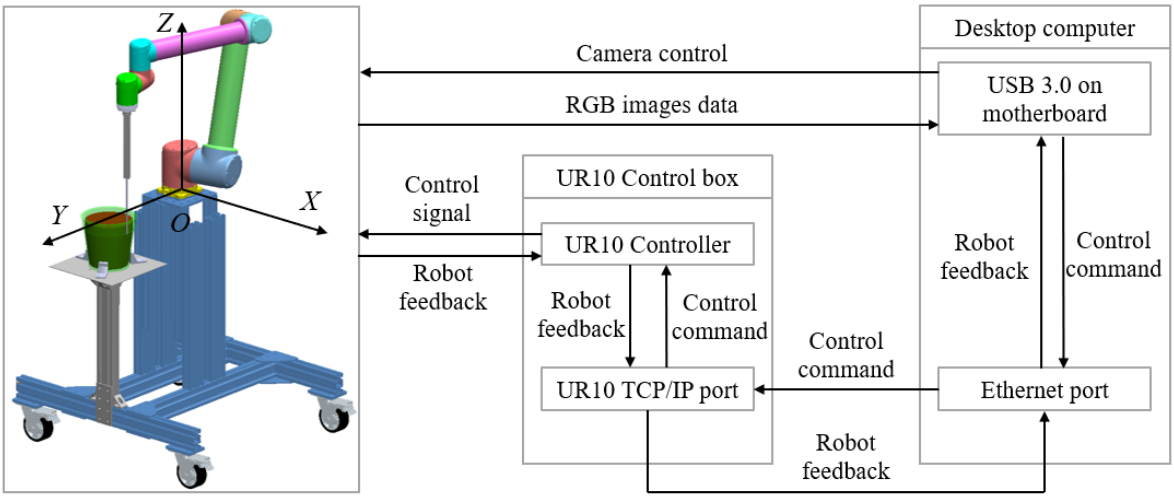

Fig. 3. System control and data flow design of MISIRoot system.

On the computer, there are 2 main scripts working together in order to complete the task. One is a sampling points generator for users to virtually mark sampling points in a pot. It takes user's experiment requirements as arguments and generates two CSV files containing the coordinates of all the sampling points and the imaging configuration parameters, such as sampling range and sample labels. The other script is the main controlling program that loads both CSV files and controls the robotic arm according to the configuration parameters. When the main control script is running, the computer forwards commands to the robotic arm, reads feedback signals from the robotic arm, controls the camera to take images, and organizes the images together with their corresponding coordinates into local files. More details of the processing logic in the program are described below.

In general, at the beginning of an experiment, the sample pot must be mounted on the experiment platform. Then, the user must manually calibrate the relative coordinate system in the control script by typing the X, Y and Z coordinates of the location where plant stem's center line intersects with the soil surface. The system coordinate orientation is shown in Fig. 3. As for the parameters required to run the system, for examples, the "Maximum sampling diameter" determines the total range of measuring. The "Plant stem diameter" indicates the region of plant stem to avoid collision between the plant and robotic arm. "Safety distance between points" and "Diameter of the camera head" are parameters used for determining the density of sampling points. The mapping algorithm ensures that all sampling points stay at least a certain distance from each other and away from the plant stem. Smaller sampling density can reduce the sampling time for each pot and reduce this system's disturbance on the soil environment, but the chance of being able to find root images may decrease.

2.1 Sampling points generator

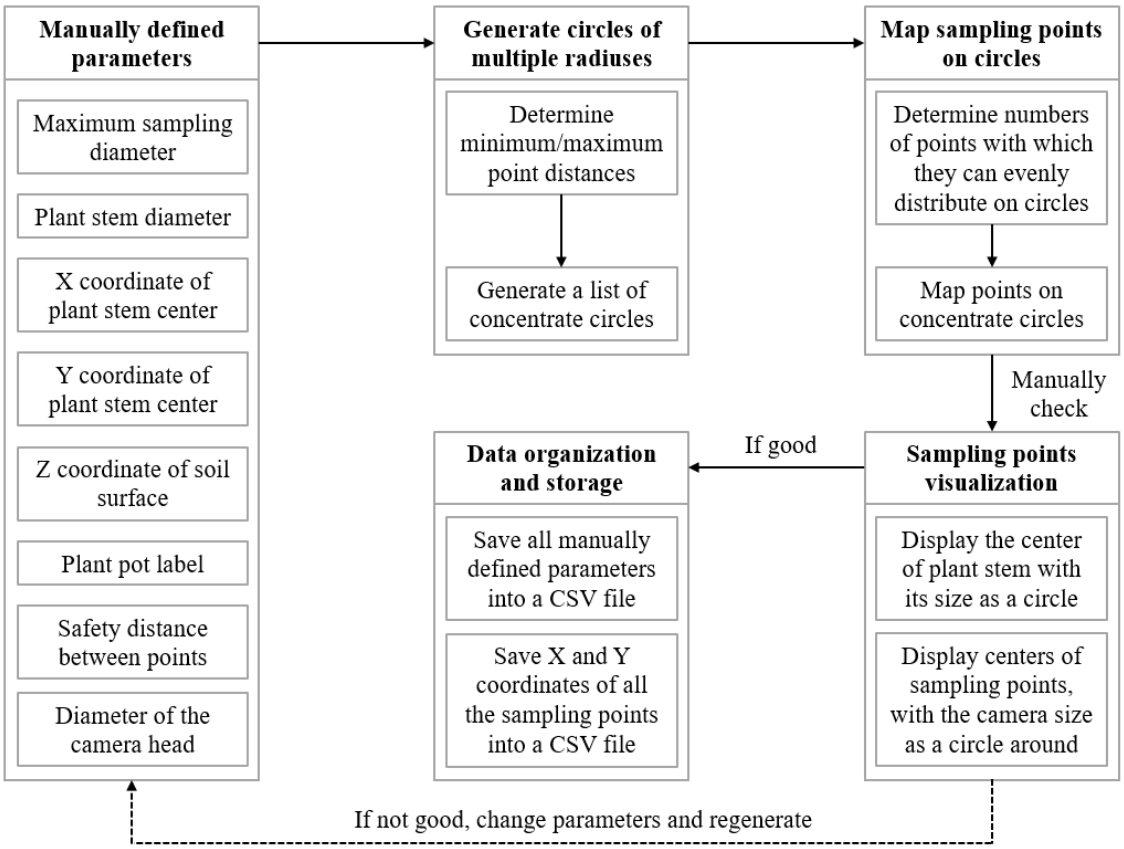

Fig. 4. A basic working flow of the sampling points generator

A basic working flow of the sampling points generator is shown in Fig. 4. Based on the user-defined parameters, the script first generates a series of virtual circles centered at the plant stem with evenly distributed radius. Then, each of the full virtual circles is evenly divided into small pieces of arcs. Edges of those arcs are tagged as sampling points and their coordinates are all recorded. All sampling points should have similar spatial interval on each virtual circle, with a possible difference within ±2 mm, which is a tolerance configuration to ensure the existence of a solution that satisfies all the requirements. Results of this script include a sampling field graph, by visualizing all sampling points, position of the plant stem, and camera's field of view at each point. The user can evaluate the experiment settings by checking this graph and tune the parameters accordingly. An example of a visualized sampling filed is shown in Fig. 5.

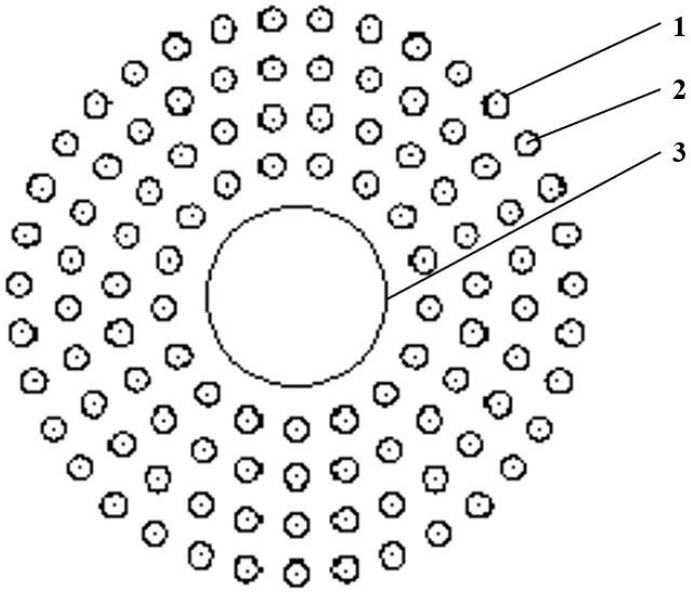

Fig. 5. An example of visualized sampling field, including the centers of all sampling points, corresponding camera's field of view, and the plant stem.

1. Camera field of view
2. Sampling points center
3. Plant stem indicator

2.2 Main controlling program

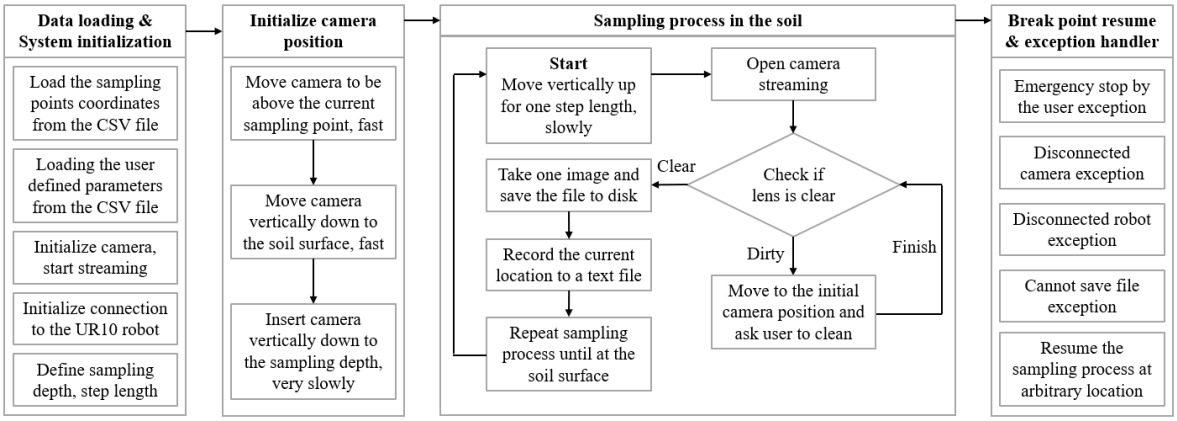

Fig. 6. A basic working flow of the main controlling program

The controlling program assumes that the two CSV files generated from the sampling points generator are ready in the computer. Fig. 6 shows the working flow of the main controlling program. The script starts with loading data files and initializing system. Then, the script generates a series of viewpoints along the Z axis for each of the sampling points. An example graph in Fig. 7. shows how the viewpoints are distributed based on the sampling points.

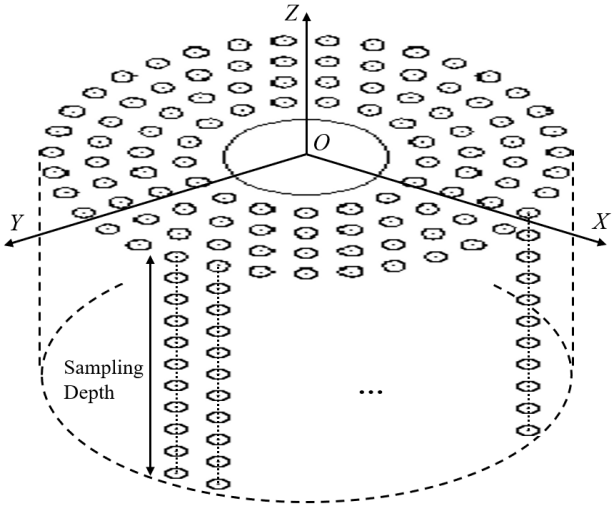

Fig. 7. An example of visualized viewpoints along the depth direction, generated based on all the sampling points generated in the previous step

Once successfully passing all the system checking procedures, the script starts the measurement process. First, in the 'Initialize camera position' stage, the robotic arm is controlled to move the camera head to the position above the first sampling point. Then, it inserts the camera head into the soil until reaching the bottom of the sampling range. This step creates a small tunnel of about 5 mm diameter in the soil. While the camera is moving up along the tunnel, the system starts the "Sampling process" stage. When the camera arrives at each viewpoint, it takes one image, record its coordinates, and save the data into local files.

To ensure high throughput and reduce as much labor time as possible, the whole sampling process control was designed to be fully automatic. In the sampling process, camera is controlled to move up step by step from the bottom of the tunnel and pauses for around 0.5 seconds at each viewpoint until finishing the imaging. At the same time, the computer keeps reading the robotic arm's position at 50Hz of frequency to check if the camera head has arrived at the correct position. Once arriving at each sampling position, the computer captures one image and saves the image and the set of 3D coordinates into local files. After completely sampling through a tunnel, the camera is moved to the initial position above the next sampling point and the system repeats the sampling process until finishing through all the sampling points. Exceptional circumstances during the sampling process such as having too much counter-acting force or moving out of safety region, will cause the system to enter the emergency-stop stage so that basic safety is ensured for automatic operation.

3. Validation experiment

A plant assay experiment was designed and conducted in June 2019. All the experimental plants were grown in one room of the greenhouse at Lilly Hall, Purdue University, West Lafayette, USA.

3.1 Validation experiment on MISIRoot's data collection quality

Several groups of plants were grown to check if the data collected from the MISIRoot could tell the differences about root growing phenotypes at different plant stages, or under different watering treatments. A total of 18 corn plants (genotype: B73 x Mo17 hybrid) were grown simultaneously for this research project. All plants had the same type of soil, which was commonly used in the greenhouse to grow corn, made by a mixture of sands and 'grow mix' (ScottMiracle-Gro Inc, USA). Plants were grown without any nutrient treatment, but with different water treatments in plastic pots (around 160 mm bottom diameter, 220 mm top

diameter, 210 mm depth, ContainerSupply Co. Ltd, China). Soil were filled into the pot to the same depth of around 165 mm, and the corn seeds were planted at the pot center with depth of about 10 mm from the soil surface. This strict seeding standard ensured that all the roots could grow from the same position and had the same amount of free space for growing roots.

Eighteen samples were equally divided into 2 main groups based on 2 levels of water treatments: well-watered group and drought-stressed group. Each group was then equally divided into 3 subgroups: V3, V4, and V5. For the well-watered group, all plants were watered with about 600 milliliters of water every 2 days after germination to keep the average soil moisture content at around 30%. For the drought-stressed group, all plants were watered with about 300 milliliters of water every 4 days after germination and the average soil moisture content was kept below 10%. The name of each subgroup indicated the stage when plants should be measured by the MISIRoot system. For example, all plants in the V3 group were measured when the plants were at the V3 stage.

Around 4 weeks after germination when the plants grew to the V3 stage, the 6 pots from V3 subgroup of both well-watered and drought-stressed groups were transported to the MISIRoot system for measuring. About 5 days after when the corn plants grew to a higher stage (V4), the 6 pots of the V4 subgroup were measured with the same sampling process as V3. The same process was utilized for plants in the V5 subgroup. With this setup, by comparing the plants at different stages with the same water treatment, root structure differences between plant stages were evaluated. By comparing the plants that are at the same stage, but with different water treatments, root structure differences caused by water conditions were evaluated.

3.2 Test of MISIRoot's influence on plant growth

Another experiment was designed to evaluate MISIRoot's impact on plant growth. In addition to the 18 plants described above, another 20 corn plants were grown for evaluating the system's disturbance to the plant growth. Similarly, all the plants were equally divided into 4 subgroups: 'Controlled well-watered', 'Controlled drought-stressed', 'Measured well-watered' and 'Measured drought-stressed', with 5 plants in each. They all had the same type of soil, same type of pot, same watering criteria, and the same genotype of corns as the 18 plants described above. At the end of the assay, the 'Controlled' plants were compared with the 'Measured' plants so that the disturbance caused by MISIRoot system could be measured in both well-watered and drought-stressed conditions. In the 'Measured well-watered' and 'Measured drought-stressed' subgroups, when plants grew to every stage of V3, V4, V5 and V6, the MISIRoot system was used to take measurement on each plant with the same sampling parameters used in the 18 pots experiment described above. Plants in 'Controlled well-watered' and 'Controlled drought-stressed' subgroups were left for growing normally without being measured by the MISIRoot system. Right after each measurements taken by MISIRoot, all 20 plants were imaged by a hyperspectral imaging station at the Lilly Hall Greenhouse of Purdue University (22). The average Normalized Difference Vegetation Index (NDVI) was determined to be a standard index to evaluate the rough health condition of green plant leaves (23). For each plant, first, all the plant body pixels were segmented from the hyperspectral image. Second, the NDVI value for each pixel was calculated with Eq. (1), in which NIR means the intensity reading at the near infrared light (800 nm), and Red means the intensity reading at red light (650 nm). Finally, the mean NDVI value of all the plant body pixels was used for comparation.

$$NDVI = \frac{NIR - Red}{NIR + Red} \quad (1)$$

By comparing the 'Controlled' subgroups and the 'Measured' subgroups, the influences on plant growth made by the measurement activities of MISIRoot system were evaluated.

3.3 Control program setup

In the experiment, some parameters varied and should be updated according to different plants such as the plant stem diameter, pot label, and stem center position. Some parameters were controlled as constants throughout the whole experiment, and they are listed in the Table 3.

Table 3. Constant parameters used for setting up the measurements in sampling points generator and the main controlling program

Parameters	values
Measuring depth (Z direction)	81 mm
Measuring step (Z direction)	3 mm
Sampling range (X-Y plane)	120 mm
Safety distance from plant stem surface	7 mm
Sampling points center distance range	8~12 mm
Camera diameter	4 mm

3.4 Preliminary data processing

Not all the images collected through this system contained plant roots. Thus, all the raw images were manually checked and classified into two classes: 'Has Root' class, and 'No Root' class. To determine the classification results, a voting rule was established which requires the 3 research team members to vote for the visibility of roots in each image.

Manual classification on a large number of images costs human labor and can be time consuming. Thus, a machine learning model was developed for the purpose of image classification based on a deep convolution neural network so called “Inception V3” (24). The model was built and trained in PyTorch 0.4.1 (25) with those manually classified images. Using a computer model to process the images can dramatically reduce the labor requirement and improve the overall throughput. The model is still under refinement and more details will be published in another separate paper.

The set of X, Y and Z coordinates of each image was recorded based on the global coordinate system relative to the robotic arm’s origin. For analyzing the data, all coordinates were transformed to the local coordinates relative to the center of the plant stem. Coordinate transformation process in form of matrix is shown in Eq. (2). The center coordinates of the plant stem were acquired when calibrating the robotic arm at the beginning of measurements on a plant.

$$\begin{bmatrix} X_{local} \\ Y_{local} \\ Z_{local} \end{bmatrix} (mm) = \begin{bmatrix} X_{stem} \\ Y_{stem} \\ Z_{stem} \end{bmatrix} (mm) - \begin{bmatrix} X_{global} \\ Y_{global} \\ Z_{global} \end{bmatrix} (mm) \quad (2)$$

Results and Discussion

System setup in real-world

Fig. 8. shows the system setup in a laboratory in Lilly Hall at Purdue University. The overall occupied space was around 1.5 meters in width, 1.5 meters in length, and 2 to 3 meters in height. Total cost of the whole system was less than $50,000. After setting up the system in the lab, a series of safety settings were configured on the main control box to fit in the working

343 environment. This system can be easily moved to a greenhouse, but the safety settings would
344 need to be reconfigured to accommodate the change in working environment.

Fig. 8. The real-world setup of the MISIRoot system in the experiment lab room at Lilly Hall, Purdue University

345

346 **Data acquisition and pre-processing**

347 As part of the preliminary image classification results, some example images of both
348 classes are shown in Fig. 9. The red bounding box in each image indicates the view and location
349 of a plant root voted by the research team members. After the manual classification, only the

images that were classified as ‘Has Root’ along with their corresponding 3D coordinates were used for further analysis.

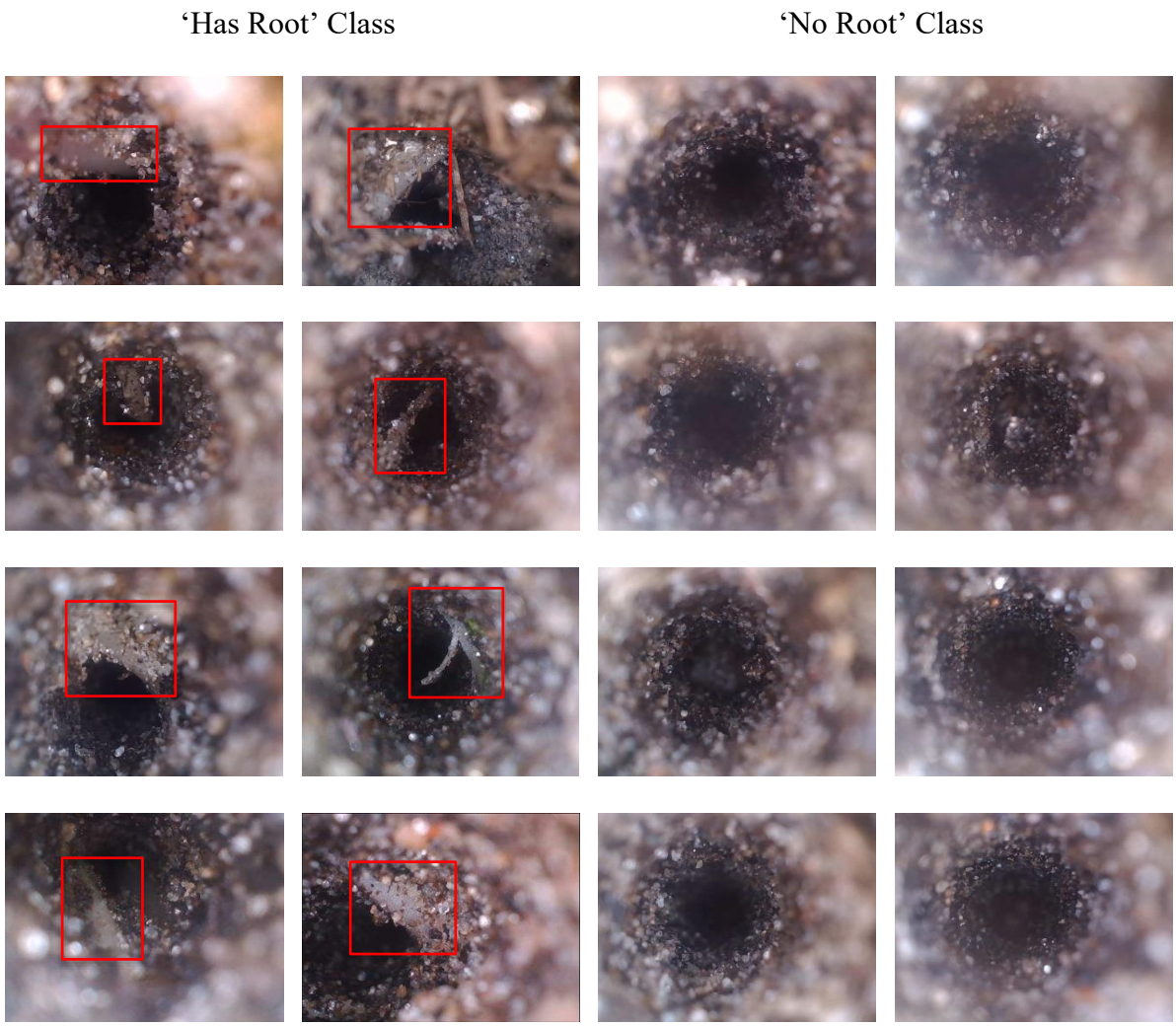

Fig. 9. Example images in both the ‘Has Root’ class and the ‘No Root’ class. Red bounding box shows the rough position where a root was identified by the team members.

In this experiment, MISIROOT was configured to have a high sampling density which resulted in about 2 hours spent and 5125 images collected for each pot. 92250 images were acquired during the whole experiment. After checking through all the images, a total of 788

images were manually labeled as the ‘Has Root’ class and were used for the further morphological analysis. The distribution of the classification resulted in the groups and subgroups are shown in the Table 4.

In order to automate the root identification process, the manually labeled images were then used to train an image classification model. Another 788 images were randomly picked from all the ‘No Root’ class images so that the data in both classes could be balanced in the dataset. Certain numbers of images were randomly picked from each of the two classes to form subgroups of data in the process of model development. There were 550 images for training, 119 images for validation and 119 images for testing (never seen by the model).With the most recent model, 108/119 (90.8%) images and 106/119 (89.1%) images in the testing dataset were correctly classified into ‘Has Root’ class and ‘No Root’ class, respectively. On the MISIRoot’s controlling computer with a normal Core-i5 CPU, and a GTX 1080 GPU, the image classification speed was around 0.05 seconds per image. This model provided an automatic, high-accuracy and fast root identification software solution in MISIRoot system.

With the 0.2 m measurement range in diameter and the 0.08 m measurement depth, the overall measurement volume inside the soil is 2.51×10^3 cm^3. Since all the sample points were evenly distributed, it was assumed that all the roots within this space had the same chance to be captured by the MISIRoot. Thus, the more roots that existed in the pot, the more ‘Has Root’ class images that were expected to be found in a pot. According to Table 4, if comparing the samples with the same treatment but at different stages, the average number of ‘Has Root’ class images increased along with the maturity of plants. It matches a common expectation that plants tend to develop more roots as they grow.

Table 4. Average numbers of 'Has Root' class images of all subgroups in both well-watered and drought-stressed groups of samples

Treatment groups	Plant stage subgroups	Average number of 'Has Root' images per pot
Well-watered	V3	30
	V4	37
	V5	61
Drought-stressed	V3	25.3
	V4	42.3
	V5	67

381

382 **Distribution of the 3D point cloud along Z axis**

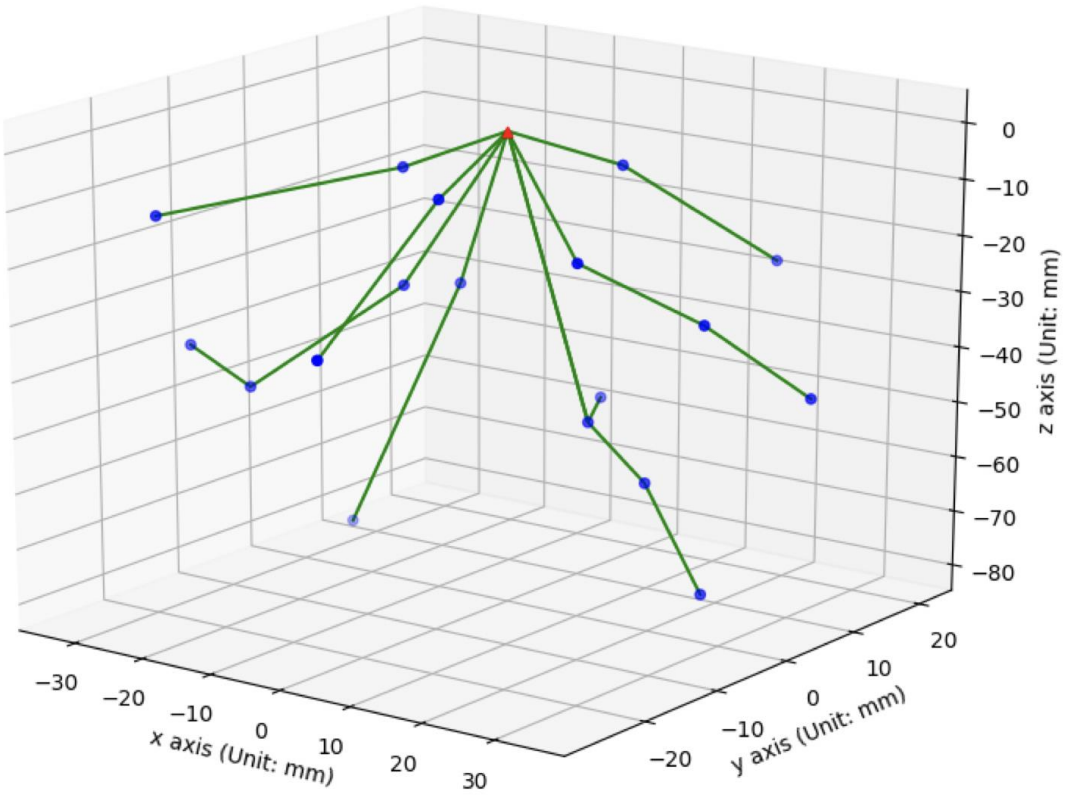

Fig. 10. An example of the points cloud generated from one plant picked from drought-stressed group at V3 stage.

1. Red triangle at the top: Seed location in the soil.
2. Blue dots: The positions where at each a root was found.
3. Green lines connected between blue dots: Possible root connections.

383

384 Fig. 10 shows an example of the 3D points cloud reconstructed with the data collected
385 from one corn plant in the drought-stressed group at V3 stage. The red triangle on the top of
386 the graph indicates the seed location in the soil. Each blue dot indicates a position at which a
387 'Has Root' class image was found. Green lines are the possible connections between cloud
388 points, showing a possible root network in the soil. The connections in this graph were
389 generated by our preliminary intuitive 3D reconstruction algorithm which connects the nearest
390 neighboring points while minimizing the turning angle at each point.

391 In order to verify the reconstruction results, the plants were scanned by an X-CT system
392 and then the roots were also washed out of the soil for observing. However, the CT images
393 were not clear enough to recognize the roots because of CT's high requirements on the soil's
394 properties. After being dug out and without the physical supports of soil, roots' original shapes
395 and structures were totally lost.

396 However, the validity of the 3D points cloud and 3D reconstruction results were proved
397 by their ability of clearly differentiating the roots from different watering treatments: The
398 calculated root size and depth results from the MISIRoot system showed significant differences
399 between the watering treatments. More specifically, a preliminary analysis was conducted
400 based on the depth distribution of those points clouds. Point cloud distribution along the Z axis
401 was analyzed. After combining all the data points of the 3 replicates within each subgroup, the
402 average depth values are shown in Fig. 11. The average root depth increased with the growing

of plant in the drought-stressed group but remains almost the same in the well-watered group. It showed that the roots in the drought stress condition were trying to grow deeper to increase their chances to survive and the roots that had enough water tend to accumulate in a relatively shallower region (5,26).

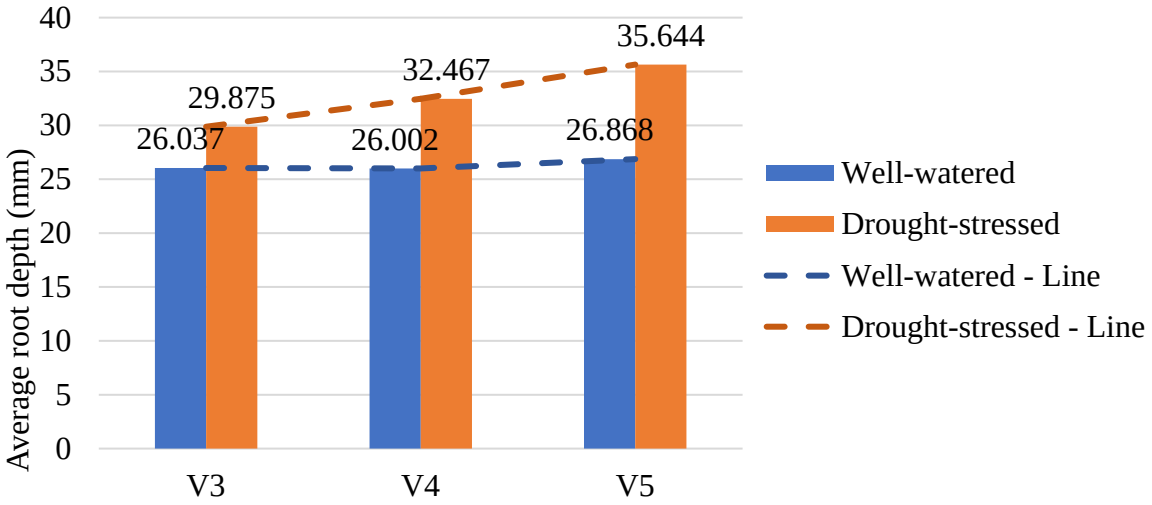

Fig. 11. The average depth values of all data points that were classified as 'Has Root' class for all treatment and stages subgroups.

The depth distributions of all subgroups are shown with boxplots in Fig. 12. Roots grew from seeds close to the soil surface, which is why the minimum depth values in all groups are close to 5 mm. Many differences between the groups can be observed from the boxplots. For example, plant roots in the drought-stressed group had larger values in both maximum depth and average depth than the well-watered group at V3 stage. In the drought-stressed group, the maximum values remained at around 80 mm which was the deepest measuring range setting for this experiment. In the well-watered group, the maximum depth was larger in the higher stage plants, but the average depth remained at a smaller value than the drought-stressed group. One hypothesis is that plants at the same stage but with different water treatments tend to have different root depth distributions (27). Because the data were not normally distributed and data transformation couldn't solve the data skewing problem, a nonparametric test should be used

in this case. To verify this hypothesis, a Kruskal-Wallis ANOVA (28) test was conducted. It tests the differences between pairs of samples at the same stage in well-watered and drought-stressed groups. The P-values are 0.2742, 0.00602, and 4.44e-6, for V3, V4, and V5 pairs respectively. To draw a preliminary conclusion for this test, at 95% significance level, the plants at V3 stage didn't show a significant difference on the depth distribution between drought-stressed group and well-watered group. However, at V4 and V5, the depth distribution difference between the plants in drought-stressed group and well-watered group was significant.

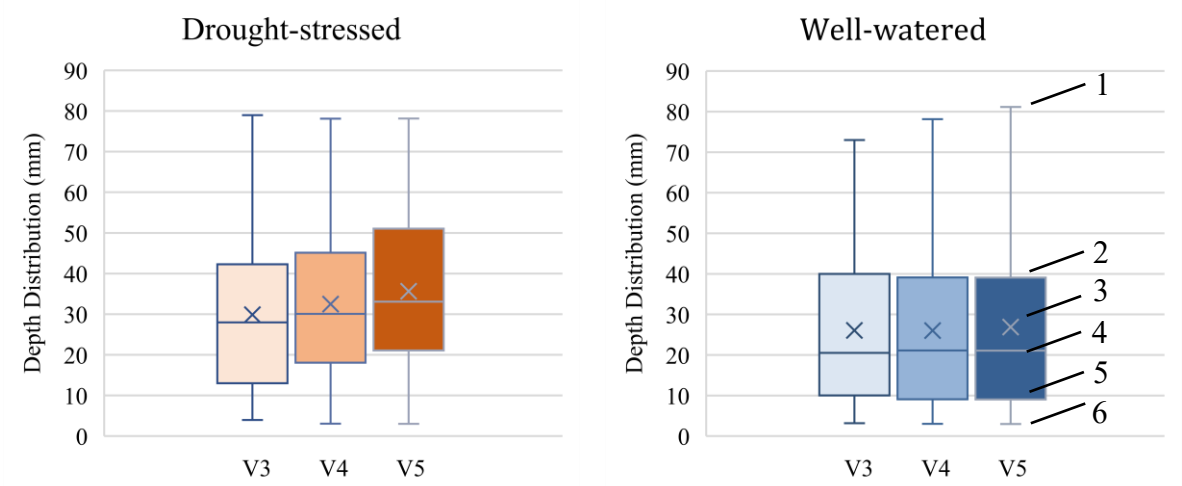

Fig. 12. The distribution of the depth values in boxplots of all subgroups. Drought-stress and well-watered groups demonstrated different growing patters in terms of the roots' depth distributions. 1: Maximum. 2: Median of the 3rd quantile. 3: Mean. 4: Median. 5: Median of the 1st quantile. 6: Minimum.

The depth distributions of all subgroups are shown in Fig. 13 with more details than the boxplots. As the plants grow and develop, plants in the drought-stressed group tended to grow more roots in a relatively deeper region (30mm ~ 70mm) but remained similar densities in the shallower (0 ~ 20mm) regions. However, plants in the well-watered group tended to grow more in the shallower regions (0 ~ 30mm) but tended to grow less in the deeper regions (> 30mm).

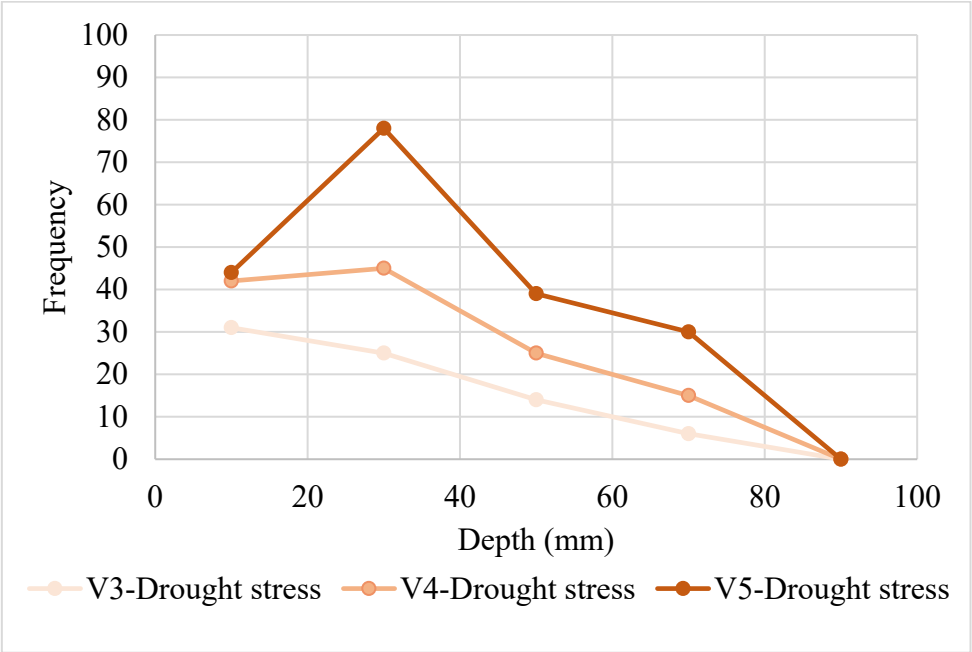

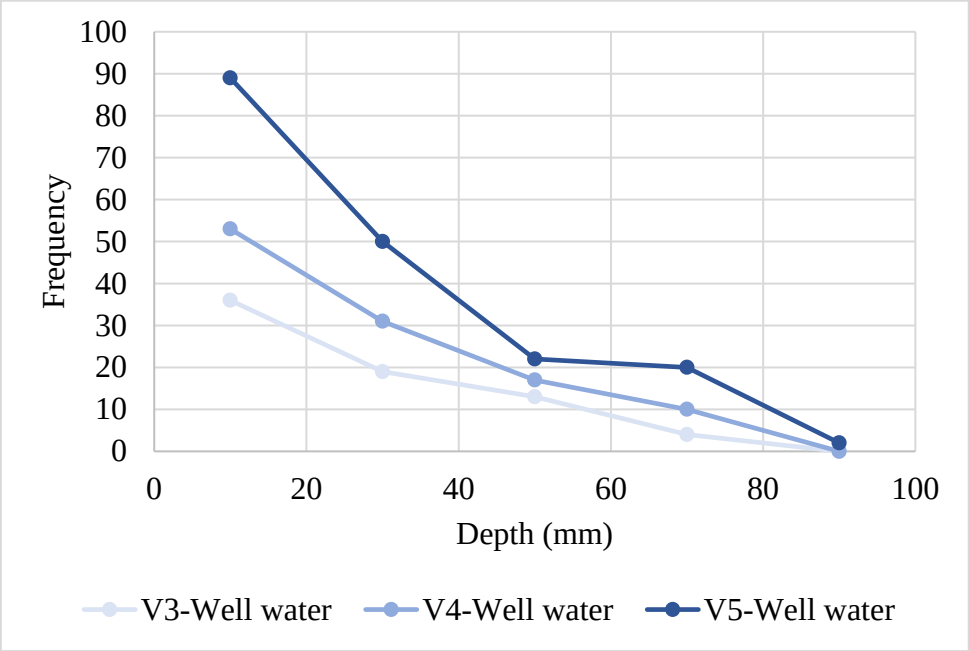

Fig. 13. Frequencies of the cloud points in both drought-stressed, and well-watered groups that fell in certain depth intervals.

Proof of minimally invasive characteristic

The NDVI values that were calculated based on the hyperspectral images of the corn plants are shown as boxplots in Table 6. The P-values of two-tailed T-tests between all pairs of control and measurement subgroups are also listed in the Table 6. The null hypothesis was

that the NDVI values of two test groups had the same mean value, while the alternative hypothesis was that the NDVI values of two test groups had different mean values. Since all the P-values are larger than 0.05, the null hypothesis was rejected at a 95% significance level. As a conclusion, utilization of the MISIRoot system did not cause significant difference on the plant growth in this experiment.

Table 5. NDVI distributions of all subgroups, and two-tailed T-test P-values between control subgroups and measurement subgroups. (a) Average NDVI values at V4 stage. (b) Average NDVI values at V5 stage. (c) Average NDVI values at V6 stage.

'C-L': 'Controlled drought-stressed' subgroup.

'M-L': 'Measured drought-stressed' subgroup.

'C-H': 'Controlled well-watered' subgroup.

'M-H': 'Measured well-watered' subgroup.

Boxplots	Test groups	T-test P-values
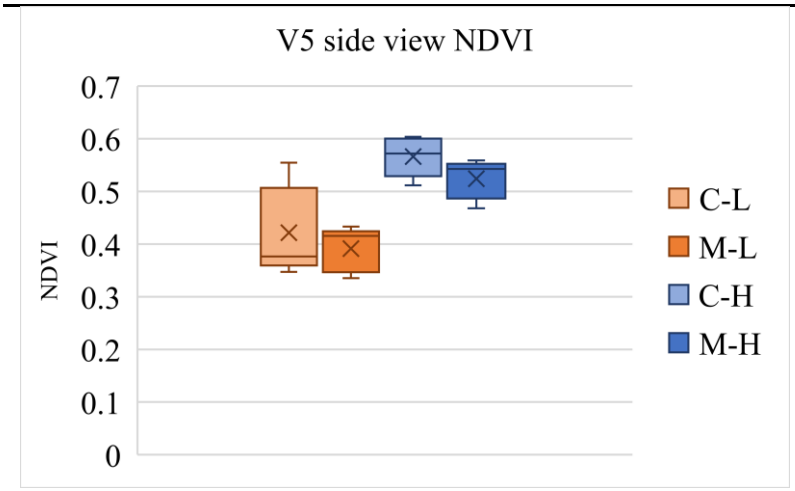 (a)	'C-L' and 'M-L'	0.593
	'C-H' and 'M-H'	0.111

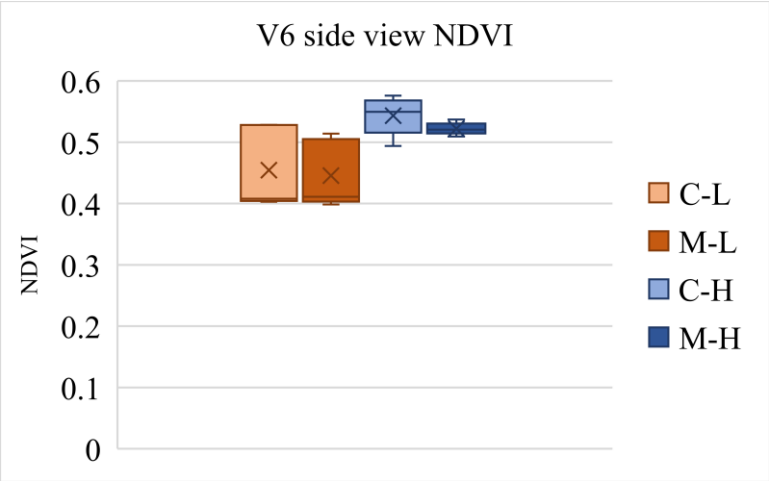

‘C-L’ and ‘M-L’	0.810
‘C-H’ and ‘M-H’	0.245

(b)

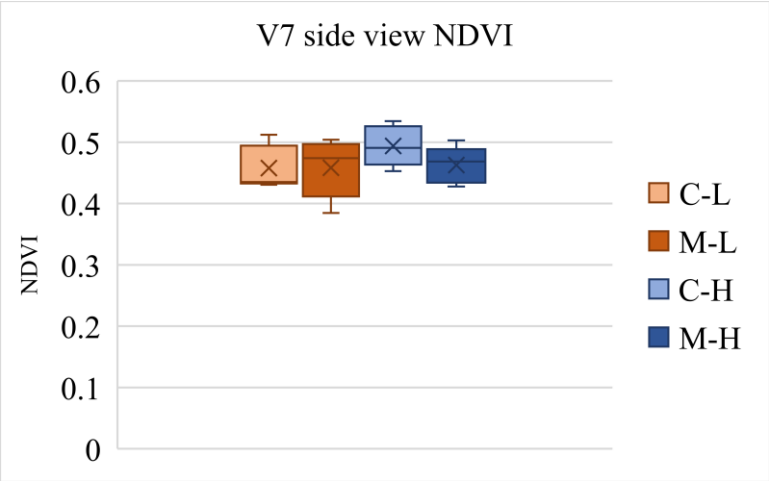

‘C-L’ and ‘M-L’	0.987
‘C-H’ and ‘M-H’	0.300

(c)

Conclusions and future work

In this study, a novel robotic imaging system, MISIRoot, was developed at Purdue University for high quality root phenotyping. MISIRoot uses a robotic arm to repeatedly insert a miniature camera into the soil while recording the real-time 3D positions and images of the roots. With a comparatively low cost, this system can automatically measure the roots’ 3D structures and take color images of the corn plant roots in normal soil, and in situ. In the most recent experiment on corn plants, MISIRoot successfully detected the roots’ significant size

and depth differences between plants at different stages and with different water treatments. In the controlled test, it was proved that the measurement activity by MISIRoot does not inhibit plant growth. There was no statistically significant difference ($\alpha = 5\%$) on the plants' average NDVI values caused by MISIRoot's measurements. This nondestructive method makes it possible to continuously monitor the growth of plant roots.

The Purdue engineering team is still working to improve MISIRoot. Future works should generalize this method with other plant roots such as soybeans. Further experiments will be conducted to evaluate the system's impact on plant growth from other aspects other than only NDVI values. When the X-CT scanner becomes available at Purdue University, X-CT root images will be collected as the ground truth to improve the current root reconstruction algorithm.

Abbreviations

X-CT: X-ray computed tomography; MRI: Magnetic Resonance Imaging; NDVI: Normalized Difference Vegetation Index.

Declarations

Ethics approval and consent to participate

Not applicable

Consent for publication

All authors have given consent for the publication.

Availability of data and materials

The original research data and process records are available from the corresponding authors on request.

Competing interests

A provisional patent application has been filed by Purdue University on the related design and development work.

Funding

The project was funded by Purdue University.

Authors' contributions

The core idea of this method was conceived by ZS and JJ. The system hardware was designed together by ZS, QW and JJ. All the computer processing script and the hardware assembly was developed and finished by ZS. The experiment preparation work was done by QW and assisted by ZS and JJ. All authors have read and approved the final manuscript.

Acknowledgements

This work was supported by the Department of Agricultural and Biological Engineering, Purdue University. The authors would like to thank Tao Wang (visiting scholar, Zhejiang University), Shelby Gruss (graduate student, Department of Agronomy, Purdue University), Dongdong Ma, Yikai Li, Ziling Chen, Jialei Wang, Tanzeel Rehman (graduate students, Department of Agriculture and Biological Engineering, Purdue University), Dr. Liangju Wang

(post-doc, Department of Agriculture and Biological Engineering, Purdue University) for their assistance and advices in the hardware manufacturing, data processing and plant management.

References

1. Cobb JN, DeClerck G, Greenberg A, Clark R, McCouch S. Next-generation phenotyping: Requirements and strategies for enhancing our understanding of genotype-phenotype relationships and its relevance to crop improvement. Vol. 126, Theoretical and Applied Genetics. 2013. p. 867–87.
2. Yang W, Duan L, Chen G, Xiong L, Liu Q. Plant phenomics and high-throughput phenotyping: Accelerating rice functional genomics using multidisciplinary technologies. Vol. 16, Current Opinion in Plant Biology. 2013. p. 180–7.
3. Paez-Garcia A, Motes C, Scheible W-R, Chen R, Blancaflor E, Monteros M. Root Traits and Phenotyping Strategies for Plant Improvement. Plants [Internet]. 2015 Jun 15 [cited 2020 Jan 7];4(2):334–55. Available from: http://www.mdpi.com/2223-7747/4/2/334
4. Zarebanadkouki M, Meunier F, Couvreur V, Cesar J, Javaux M, Carminati A. Estimation of the hydraulic conductivities of lupine roots by inverse modelling of high-resolution measurements of root water uptake. Ann Bot [Internet]. 2016 Oct [cited 2020 Jan 7];118(4):853–64. Available from: https://academic.oup.com/aob/article-lookup/doi/10.1093/aob/mcw154
5. Uga Y, Sugimoto K, Ogawa S, Rane J, Ishitani M, Hara N, et al. Control of root system architecture by DEEPER ROOTING 1 increases rice yield under drought conditions. Nat Genet. 2013 Sep;45(9):1097–102.
6. Hashiguchi Y, Tasaka M, Morita MT. Mechanism of Higher Plant Gravity Sensing. Am J Bot [Internet]. 2013 Jan [cited 2020 Jan 7];100(1):91–100. Available from:

519 http://doi.wiley.com/10.3732/ajb.1200315
520 7. DREW MC. Sensing soil oxygen. Plant, Cell Environ [Internet]. 1990 Sep [cited 2020
521 Jan 7];13(7):681–93. Available from: http://doi.wiley.com/10.1111/j.1365-
522 3040.1990.tb01083.x
523 8. Crook MJ, Ennos AR. Stem and Root Characteristics Associated with Lodging
524 Resistance in Four Winter Wheat Cultivars. J Agric Sci. 1994;123(2):167–74.
525 9. Ryan PR, Delhaize E, Watt M, Richardson AE. Plant roots: Understanding structure and
526 function in an ocean of complexity. Ann Bot. 2016;118(4):555–9.
527 10. Cheol Song G, Sim H-J, Kim S-G, Ryu C-M. Root-mediated signal transmission of
528 systemic acquired resistance against above-ground and below-ground pathogens. Ann
529 Bot [Internet]. 2016 Oct [cited 2020 Jan 7];118(4):821–31. Available from:
530 https://academic.oup.com/aob/article-lookup/doi/10.1093/aob/mcw152
531 11. De Baets S, Poesen J, Reubens B, Wemans K, De Baerdemaeker J, Muys B. Root tensile
532 strength and root distribution of typical Mediterranean plant species and their
533 contribution to soil shear strength. Plant Soil. 2008;305(1–2):207–26.
534 12. Iyer-Pascuzzi AS, Zurek PR, Benfey PN. High-Throughput, Noninvasive Imaging of
535 Root Systems. Methods Mol Biol [Internet]. 2013;959(2):247–64. Available from:
536 http://link.springer.com/10.1007/978-1-62703-221-6
537 13. Clark RT, MacCurdy RB, Jung JK, Shaff JE, McCouch SR, Aneshansley DJ, et al.
538 Three-dimensional root phenotyping with a novel imaging and software platform. Plant
539 Physiol. 2011;156(2):455–65.
540 14. Amato M, Lupo F, Bitella G, Bochicchio R, Abdel Aziz M, Celano G. A high quality
541 low-cost digital microscope minirhizotron system. Comput Electron Agric [Internet].
542 2012;80:50–3. Available from: http://dx.doi.org/10.1016/j.compag.2011.10.014
543 15. Pateña G, Ingram KT. Digital acquisition and measurement of peanut root minirhizotron

images. Agron J. 2000;92(3):541–4.

16. Lu W, Wang X, Wang F. Adaptive minirhizotron for pepper roots observation and its installation based on root system architecture traits. Plant Methods [Internet]. 2019;15(1):1–14. Available from: https://doi.org/10.1186/s13007-019-0414-z

17. Mairhofer S, Zappala S, Tracy S, Sturrock C, Bennett MJ, Mooney SJ, et al. Recovering complete plant root system architectures from soil via X-ray μ-Computed Tomography. Plant Methods [Internet]. 2013 Mar 20 [cited 2019 May 21];9(1):8. Available from: http://plantmethods.biomedcentral.com/articles/10.1186/1746-4811-9-8

18. Mooney SJ, Pridmore TP, Helliwell J, Bennett MJ. Developing X-ray computed tomography to non-invasively image 3-D root systems architecture in soil. Vol. 352, Plant and Soil. 2012. p. 1–22.

19. Pflugfelder D, Metzner R, Van Dusschoten D, Reichel R, Jahnke S, Koller R. Non-invasive imaging of plant roots in different soils using magnetic resonance imaging (MRI). Plant Methods. 2017;13:102.

20. Metzner R, Eggert A, van Dusschoten D, Pflugfelder D, Gerth S, Schurr U, et al. Direct comparison of MRI and X-ray CT technologies for 3D imaging of root systems in soil: potential and challenges for root trait quantification. Plant Methods [Internet]. 2015 [cited 2019 Nov 18];11(1):17. Available from: http://www.plantmethods.com/content/11/1/17

21. Zappala S, Mairhofer S, Tracy S, Sturrock CJ, Bennett M, Pridmore T, et al. Quantifying the effect of soil moisture content on segmenting root system architecture in X-ray computed tomography images. Plant Soil. 2013 Sep;370(1–2):35–45.

22. Ma D, Carpenter N, Amatya S, Maki H, Wang L, Zhang L, et al. Removal of greenhouse microclimate heterogeneity with conveyor system for indoor phenotyping. Comput Electron Agric. 2019 Nov 1;166:104979.

569 23. Tucker CJ. Red and photographic infrared linear combinations for monitoring
570 vegetation. Remote Sens Environ. 1979;8(2):127–50.
571 24. Szegedy C, Vanhoucke V, Ioffe S, Shlens J, Wojna Z. Rethinking the Inception
572 Architecture for Computer Vision. In: Proceedings of the IEEE Computer Society
573 Conference on Computer Vision and Pattern Recognition. IEEE Computer Society;
574 2016. p. 2818–26.
575 25. Paszke A, Gross S, Chintala S, Chanan G, Yang E, Facebook ZD, et al. Automatic
576 differentiation in PyTorch. 2017 Oct.
577 26. Hund A, Ruta N, Liedgens M. Rooting depth and water use efficiency of tropical maize
578 inbred lines, differing in drought tolerance. Plant Soil. 2009 May;318(1–2):311–25.
579 27. ZHU J, BROWN KM, LYNCH JP. Root cortical aerenchyma improves the drought
580 tolerance of maize (*Zea mays* L.). Plant Cell Environ [Internet]. 2010 Feb [cited 2020
581 Jan 8]; Available from: http://doi.wiley.com/10.1111/j.1365-3040.2009.02099.x
582 28. Ostertagová E, Ostertag O, Kováč J. Methodology and application of the Kruskal-Wallis
583 test. Appl Mech Mater. 2014;611:115–20.
584